Acoustic navigation of a large-aperture array

Barbara J. Sotirin and John A. Hildebrand
Marine Physical Laboratory, Scripps Institution of Oceanography, University of California, San Diego, La Jolla, California 92093

(Received 11 April 1989; accepted for publication 4 August 1989)

Acoustic travel time measurements were used to navigate the elements of a large-aperture (900 m) acoustic array. Array navigation system performance was evaluated during a vertical deployment in the northeast Pacific from the Research Platform FLIP. A network of bottom-moored acoustic transponders were interrogated from FLIP and their 12-kHz replies were detected by receivers at 75-m intervals along the array. A nonlinear least-squares algorithm was used to estimate FLIP and array element positions from the travel time measurements. The FLIP positions derived from this procedure agreed with positions obtained from global positioning system (GPS) satellite navigation to within a 10-m rms error. Navigated positions for FLIP were internally consistent with a 0.5-m mean rms error and standard deviation of 1.1 m, and, for an array element, were consistent with a 2.8-m mean rms error and standard deviation of 0.8 m. The resulting time series of array and FLIP motions were analyzed with respect to wind, tidal, and internal wave forcing functions. Wind and tidal forcing had the greatest influence on FLIP motion, whereas array motion was governed by FLIP movement, tides, and higher frequency sources. Low-frequency array motion, with periods on the order of hours, was a result of FLIP towing the array over a horizontal range of 300 m in response to the wind and the semidiurnal tidal oscillations; the array remained within a 30-m horizontal range of FLIP's position. Higher frequency array motion had apparent internal wave and surface-coupled components. The array shape was primarily straight and nearly vertical, to within approximately a 2° tilt, responding as a simple pendulum with small displacements.

PACS numbers: 43.30.Tg, 43.30.Pc

INTRODUCTION

Large-aperture arrays produce high-resolution directional information by coherently combining signals from individual array elements. Estimates of array shape and element position are required because of the dependence of signal phase on element location. Navigation of such an array in the ocean requires a known reference system in a spatially and temporally varying environment.

A 900-m, 120-element low-frequency acoustic array has been developed by the Marine Physical Laboratory.[1] The array is capable of being deployed either horizontally or vertically up to an ocean depth of 6000 m. Navigation of the array is an important part of its operational requirements, and the subsystem implemented to perform the navigation must meet design specifications. The position accuracy required is on the order of a a few meters, the duration of deployment is on the order of a few months, an operating range of up to 10 km must be viable, the size and cost of the system must be manageable, and the sampling rate must be sufficient to resolve array dynamics due to water currents, tides, wind, and internal waves.

Techniques commonly used in ocean positioning systems are based on mechanical, electromagnetic, or acoustic signals.[2] Mechanical positioning devices capable of the accuracy required include inertial systems, pressure sensors, tilt meters, measuring rods, and sound-velocity meters. The cost and size requirements of instrumenting a 900-m array with such sensors is prohibitive, although pressure sensors would be valuable for depth positioning in combination with an alternative method for lateral positioning. Electromagnetic systems are either surface systems whose signals are highly attenuated in water, but are useful in determining the position of a surface vessel [e.g., global positioning system (GPS)], or pulsed laser systems, which are currently under development and may eventually be effective within a 1-km range. The technique most easily adapted to a large-aperture array deployed in the water column is acoustic navigation. Such systems measure the travel time of acoustic energy between two points in the ocean, are capable of resolving a few meters over a 10-km range, and are cost effective and physically manageable. Based on these considerations, an acoustic navigation subsystem was implemented as an integral part of the array.

This paper describes the array acoustic navigation system and its operation during a vertical deployment from research platform FLIP in the northeast Pacific during September 1987. We describe the hardware system and acquisition of travel time measurements and associated errors, the nonlinear least-squares estimation of array spatial positions, and the analysis of FLIP and array time-varying positions during the deployment.

I. TRAVEL TIME MEASUREMENTS

Acoustic travel time measurements provide range information between the array and a set of fixed transponders. Ranges to three or more transponders are required to calculate FLIP position and array position and shape. The navigation hardware consisted of three bottom-moored acoustic

 0001-4966/90/010154-14$00.80

transponders, two transmit/receive timing units mounted on FLIP (one used for FLIP navigation and the other used for array navigation), an interrogator/receiver located at the bottom of FLIP, and 12-kHz acoustic detectors distributed along the array. At a known time, an interrogation signal is transmitted from FLIP. This signal triggers a transponder reply, which is then detected by the array or the FLIP receiver systems. The travel times between the transponders, FLIP, and the array detectors determine array position and shape.

During the September 1987 experiment, three navigation transponders were moored in 4700 m of water distributed as a 1.4-nmi. equilateral triangle. FLIP's position was maintained in the middle of the transponder network by a three-point moor (Fig. 1). The transponders were deployed by a surface support ship operating a GPS satellite navigation receiver for absolute positional information. The transponders were equipped with anchors (175 kg) to secure them to the ocean floor and to constrain the horizontal movement during descent (sink rate of approximately 1 m/s). Once anchored, they were buoyed up above the anchor on 100-m lines with 130 kg of hard floats to limit horizontal movement and to insure a well-separated bottom bounce. They operate by detecting a unique interrogation frequency and answer with a 3-ms reply at 12 kHz with a source level of 190 dB *re*: 1 μPa at 1 m. The recognition delay time is 0.5–3 ms, depending upon the signal-to-noise ratio of the interrogation pulse.[3] Due to the proximity of FLIP, the absence of other local high-frequency ambient noise sources, and the manual control of the signal level on the interrogator, a constant delay time of less than 1 ms was assumed.

The interrogation pulse was sent from a transceiver mounted on the bottom of FLIP (90 m in depth). The pulse level was adjusted manually above the ambient noise for consistent transponder replies. The pulse was triggered by either a chart recorder to navigate FLIP or by an interrogation circuit to navigate the array. The chart recorder trace, set on a 1-s sweep rate, displayed the 12-kHz transponder reply amplitudes in a 500-Hz band with a transmit/receive delay time of 0.1 ms. Each transponder was interrogated individually to facilitate identification and transmitted a reply pulse once per second for 45 s. Since the FLIP transducer was also used as an interrogator for the array navigation system, only one system was operable at a time; consequently, the FLIP navigation data were recorded only once an hour during the sea test. Round-trip travel times for navigating FLIP were measured by hand from the chart recorder output with an estimated rms error of 2–3 ms.

The 900-m array was deployed vertically from FLIP with a 420-kg weight attached to maintain a nearly vertical orientation. The array navigation subsystem was composed of 12 hydrophones with 75-m spacing monitored by 12 individually programmable processors. Each of the 12 processors contained tuned navigation receivers designed to detect the 12-kHz transponder reply in a 200-Hz band with a -6-dB minimum signal-to-noise ratio. Once per minute the transceiver on FLIP sent out four continuous wave (cw) pulses: three transponder interrogation pulses at unique fre-

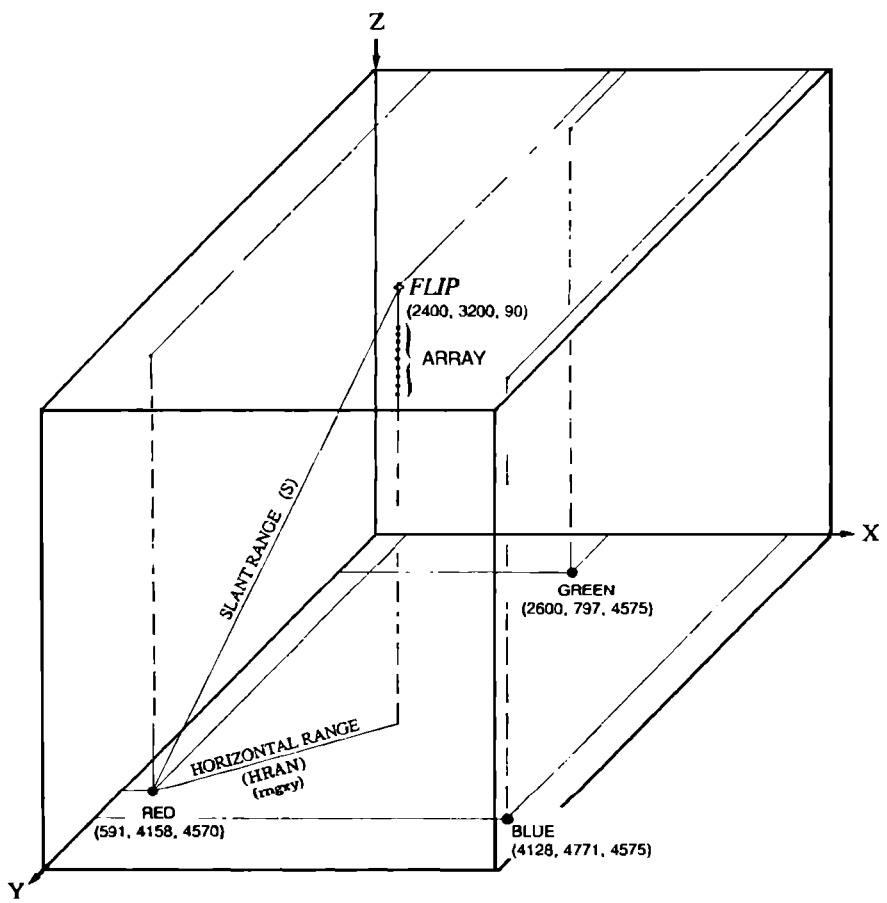

FIG. 1. Navigation overview. The navigation system consists of three bottom-moored transponders in an equilateral triangle about FLIP and the vertical array. The transponders are designated by color: red, green, and blue. The initial *xyz* coordinates of the transponders and of the FLIP interrogator are indicated.

quencies, followed by a 12-kHz pulse for depth ranging. The 12-kHz transponder replies (3 ms) and the 12-kHz depth ranging pulse from FLIP (10 ms) were recorded in series as a 1-bit output, every 0.4 ms, by each of the array navigation receivers.[4] The interrogation sequence clock was synchronized with the array time base and recorded every 128 ms.

To calculate the travel time, the time of the transponder return must be determined relative to the time of the interrogation. The signal that initiated the interrogation sequence was found by linear interpolation of the interrogation sequence clock. The leading edge of the return pulse was found by recreating each of the navigation receiver time series, and correlating these binary time series with a pulse replica that depended upon array receiver noise and level of detection. A 1-s time interval of the normalized correlation output from each array section is shown for each transponder in Fig. 2. The correlated arrival across the array of each transponder reply is evident; interference and noise are also evident. To reduce the chances of detecting a noise spike or multipath return rather than the direct transponder reply, a window was invoked, for each expected return, during which time the data were considered valid, as shown by the small $\times$'s in Fig. 2. The window was allowed to track the replies as the arrival time shifted with array movement. The travel time from the transponder to the array is the difference between the departure time of the interrogation pulse and the arrival

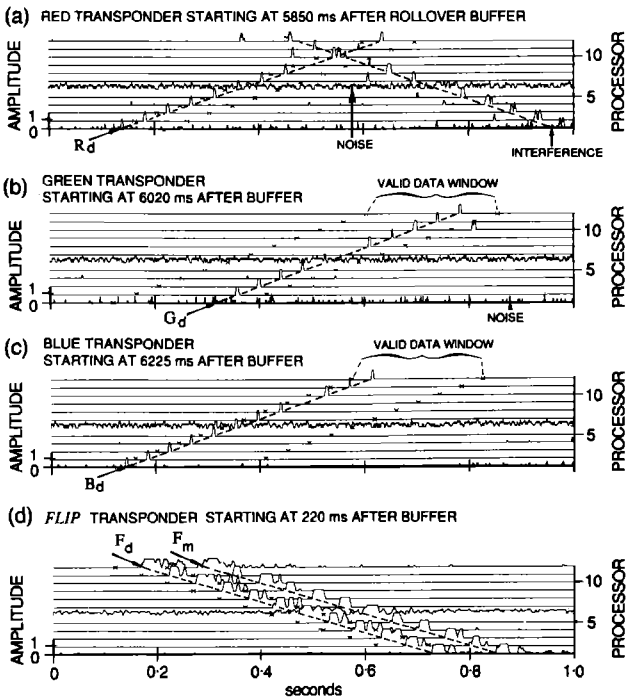

FIG. 2. Travel time acquisition. The 12 array navigation receivers each detect four pulses during a 65.536-s navigation cycle. The normalized correlated receiver outputs are shown during a 1-s interval bracketing each detection. The top trace represents the output of the top receiver, followed in sequence by the deeper receivers. The first three panels, (a)–(c), represent the detected direct replies of the three transponders (shown as R_d,G_d and B_d), arriving at the deepest receiver first and traveling up through the water column to the shallower receivers. The last panel (d) shows the detection of the direct arrival F_d of the 12-kHz pulse transmitted from FLIP traveling down the array, with a surface reflection F_m arriving about 120 ms after the direct pulse. The small $\times$'s represent the valid data window. The start time is indicated at the top of each panel.

time of the transponder reply at the leading edge of the correlated signal, minus the travel time from FLIP to the transponder and the constant system delay times.

The accuracy of the travel time measurements from the bottom transponders to the array was dependent upon factors which affected all receivers similarly as well as factors which varied with each array receiver. The factors with similar effect were: (a) the ambient ocean noise in the 12-kHz band, which has a typical level of 30–40 dB//μPa/$\sqrt{\text{Hz}}$, and (b) the transponder performance, which introduced timing errors.[4] The factors that varied with receiver were: (a) the drift in the array clock phase lock loop circuitry,[1] which introduces small sampling time errors, (b) the FLIP-to-transponder travel time measurement error (the resultant error in array-to-transponder range increases as depth decreases) of order 1.5 ms, and (c) the noise and detection threshold of the array receivers. The variation in receiver error[4] is confined for the most part to a mismatch in detection threshold due to the temperature sensitivity of the capacitors and high failure rate of the inductors in the tuned navigation filters. This variation was estimated at 2 ms during laboratory tests of the frequency sensitivity of the tuned filters and by examining the length of the transponder replies. Estimated accuracy for the array travel time measurements depends upon the receiver and the depth of the array, but is typically 2–3 ms. The accuracy of the depth measurements is affected by the ambient ocean noise, the transmitter and detector noise, the detection threshold, and the strength of the transmission. Measurement error in the travel times corresponding to array depth is estimated, by calculating the mean standard deviation in ten sample segments, to be < 1 ms.

II. POSITION ESTIMATION

In this section we determine where the three bottom transponders, the FLIP transceiver, and the array elements are in three-dimensional space using the travel times described in the previous section. The general problem of fitting model functions and parameters (spatial positions) to data (travel-times) appears in many areas of applied science: as parameter estimation, regression analysis, inverse problems, filtering, process identification, and as an optimization problem in numerical analysis. Noise in the travel time measurements demands that sufficient data be collected to overdetermine the solution, requiring some kind of approximation method.

To approximate the solution, an optimization problem is defined to minimize differences between model predictions and actual measurements. The function relating predictions and measurements is determined by the problem structure and the error distribution. One approach is to minimize the differences with respect to a matrix norm. Analytically, the most viable choice is the l_2 norm resulting in the familiar least-squares solution. If the errors are independent and distributed normally with a constant standard deviation, then the l_2 norm coincides with the maximum-likelihood solution. The least-squares solution magnifies the effect of large errors, and if the error distribution contains many outliers, the l_1 norm solution as described by Gill *et*

al.[5] and implemented by Duckworth[6] is an attractive alternative. Although the l_1 solution is more robust in terms of outliers, these errors continue to affect the solution, and if possible, the source of the large errors should be identified and removed.

The navigation problem discussed here has been implemented in terms of the least-squares method. The transponder net was localized separately to allow accurate real-time array navigation. The FLIP travel time measurements used for the transponder localization are very consistent and possess no large errors, having been selected and verified by hand. *A priori* knowledge of array measurement errors did not justify deviation from the assumed normal distribution. In the remainder of this section, a general description of the least-squares formulation is followed by the specific details of implementation for the array navigation problem. The effect of specific types of errors are simulated, and results are presented.

A. Least-squares formulation

The FLIP, array, and transponder positions were estimated by a nonlinear least-squares method. The problem is to find the set of model parameters (spatial positions), given a set of measurements (travel times) plus noise. The least-squares estimator identifies a realistic set of parameters by minimizing the sum of the squared errors, with an error defined by the difference between the model estimate and the measurement. For the set of measured data v_k (travel times), and the set of parameters a_j (spatial positions) that determine the model estimate $\hat{v}_k(a_j; j = 1,N)$ (referred to as $\hat{\mathbf{v}}$ or $\hat{v}_k$), the least-squares formulation is written as

$$\underset{\mathbf{a}\in R^N}{\text{minimize}}\left(\mathbf{F}(\hat{\mathbf{v}};\mathbf{a}) = \sum_{k=1}^{M} \frac{(v_k - \hat{v}_k)^2}{\sigma^2} = (\mathbf{v}-\hat{\mathbf{v}})^T \mathbf{R}^{-1}(\mathbf{v}-\hat{\mathbf{v}})\right), \quad (1)$$

where the measurement errors are uncorrelated with identical variances σ^2 and $\mathbf{R}$ is $\sigma^2\mathbf{I}$. The error function $\mathbf{F}(\hat{\mathbf{v}};\mathbf{a})$ (designated as $\mathbf{F}$), is minimized when the gradient $\mathbf{g}$ of $\mathbf{F}$ with respect to the model parameters is zero:

$$\mathbf{g} = \frac{\partial \mathbf{F}}{\partial \mathbf{a}} = -2(\mathbf{v}-\hat{\mathbf{v}})^T \mathbf{R}^{-1} \frac{\partial \hat{\mathbf{v}}}{\partial \mathbf{a}} = 0. \quad (2)$$

In general, a closed-formed (one-step) least-squares solution exists, provided the set of equations is linear. For the array navigation problem, however, the nonlinear mapping from measurement space to parameter space necessitates an iterative implementation. One such implementation is to approximate the smooth nonlinear functions described by $\mathbf{F}$ with a linear form of the Taylor's series expansion about an initial position $\mathbf{a}_I$. In the immediate neighborhood of $\mathbf{a}_I$,

$$\mathbf{F}(\hat{\mathbf{v}};\mathbf{a} + h\mathbf{p}) = \mathbf{F}(\hat{\mathbf{v}};\mathbf{a}_I) + \sum_{j=1}^{N} hp_j \left.\frac{\partial \mathbf{F}}{\partial a_j}\right|_{\mathbf{a}_I}, \quad (3)$$

where h is a scalar, and $\mathbf{p}$ is a direction vector guiding the search for a minimum. In terms of the iteration step the notation may be written

$$F_{n+1} = F_n + h_n \mathbf{g}_n^T \mathbf{p}_n, \quad (4)$$

where $\mathbf{g}_n$ is the gradient of $\mathbf{F}$ at $\hat{\mathbf{v}}_n$. An acceptable minimum for $\mathbf{F}$ is obtained by calculating the estimate $\hat{\mathbf{v}}$ from an initial "best guess" for the parameters $\mathbf{a}_I$, then developing a prescription which improves this initial guess, updating the parameters until specified convergence criteria are satisfied. A typical prescription to search for this minimum is to calculate $\hat{\mathbf{v}}$ from $\mathbf{a}_I$, F_n from $\mathbf{v}$ and $\hat{\mathbf{v}}_n$, and complete the following steps:

(1) Compute a vector $\mathbf{p}_n$, which is the search direction.

(2) Compute a scalar step length h_n.

(3) Update the estimate of the parameters. Set $\mathbf{a}_{n+1} \leftarrow \mathbf{a}_n + h_n\mathbf{p}_n$, followed by $n \leftarrow n+1$, such that the current error function is now F_n.

(4) Test for convergence. Calculate the forward problem, which determines current estimates $\hat{\mathbf{v}}_n$ of the measurements $\mathbf{v}$ from current estimates of the parameters $\mathbf{a}_n$. Evaluate F_n and F_{n-1} with respect to the convergence criteria. If the conditions for convergence are satisfied, the current value of $\mathbf{a}_n$ is considered the solution; if not, iterate by returning to step (1).

To implement this prescription, the choice of convergence criteria, search direction, and step length must be considered; particular choices relating to array navigation will be specified in the following section. In an optimization problem, the value at the minimum is generally not known, and convergence criteria must be developed to bound the number of iterations while insuring that the resulting solution is sufficiently close to the real minimum. Specific criteria are defined by evaluating the magnitude of the gradient, the magnitude of the squared error, and the relative decrease in squared error with respect to acceptable tolerances δ_i as follows:

$$\begin{aligned} &||\mathbf{g}_n|| < \delta_1, \\ &F_n < \delta_2, \\ &0 \leqslant F_{n-1} - F_n < \delta_3, \\ &\text{number of iterations} > 1/\delta_4. \end{aligned} \quad (5)$$

Combinations of the above criteria determine convergence. The rate of convergence depends on the specific minimization algorithm, the initial estimates, and the error surface. The resulting minimum point could be either global or local. In general, there are no sure methods for finding global minima; so the accuracy of the initial guess is important.

Consider the iterative step in the direction of search $\mathbf{p}_n$. In the univariate case, the only possible directions are positive or negative. As the number of dimensions increases, even to two, the number of possible directions is theoretically infinite. Search direction procedures are typically direct search methods or gradient search methods with the constraint that $\mathbf{p}_n$ be a descent direction. Iterative search procedures having the general form of Eq. (4) lend themselves easily to gradient search methods. To define the gradient search, if $\mathbf{g}_n$ is nonzero, there must exist a vector $\mathbf{p}_n$ such that $\mathbf{g}_n^T\mathbf{p}_n < 0$. If $\mathbf{p}_n$ is defined as $-\mathbf{g}_n$ and the gradient is nonzero, this direction is clearly a descent direction; the algorithm is recognized as the steepest descent method. It follows from Eq. (4) that, for any small positive step size h, $F_{n+1} < F_n$. Since $\mathbf{p}_n$ is in the direction of decreasing $\mathbf{F}$, con-

vergence is guaranteed provided h_n is chosen so that F is "sufficiently decreased" at each iteration. To be appropriate, h_n must be small enough to locate the minimum precisely and satisfy the immediate neighborhood constraint of Eq. (4), and at the same time large enough to search efficiently. The existence of guaranteed convergence of the algorithm does not imply that convergence will be achieved in an acceptable number of iterations. A common method used to define h is to follow the steepest descent gradient for the current iteration to a minimum. This dictates that the next search direction be nearly orthogonal to the current direction $\mathbf{g}_n^T \mathbf{p}_{n+1} \to 0$. It has been shown that the directions generated by this method asymptotically converge to only two directions for many problems,[7] increasing the number of iterations immensely. This situation may be avoided by constraining the step size to be less than that required to reach the minimum in the current search direction. Although the rate of convergence of the steepest descent algorithm is known to be less than other methods,[5] the method is numerically stable and produces efficient results for the navigation problem considered here.

B. Implementation

We discuss implementation of the general nonlinear least-squares method described above for the transponder and array navigation. The ingredients required for a least-squares problem are: (1) the measurements $\mathbf{v}$ (travel time detected at the array and at FLIP); (2) the initial estimates of the model parameters $\mathbf{a}$ represented by FLIP, array, and transponder xyz positions; (3) the mapping function from measurement space to parameter space which calculates the estimates $\hat{\mathbf{v}}$ from the parameters $\mathbf{a}$; and (4) the measurement errors $\boldsymbol{\sigma}$. Although the general prescription is the same for the transponder localization and for the FLIP/array localization, there are differences in the implementation. In the following, the explicit inputs and implementation of the transponder localization are specified and the differences relating to FLIP and the array are discussed separately.

1. Transponder localization

The two-way travel times between FLIP and the transponders were used for transponder xy position estimation. Normally, data from an extensive surface ship survey would be available for localizing the transponders.[8,9] Although such a survey was conducted during the experiment, the data were not complete due to extreme noise levels of the surface ship; instead data recorded by the FLIP navigation system were used. The FLIP data set defines a survey configuration that is not optimal; however, the extended time series and low errors of the FLIP measurements increase their reliability over the other available data sets. The unconventional geometry of these measurements imparts a rotational symmetry to the problem, as FLIP was moored in the center of a roughly equilateral triangle defined by the transponder positions. This physical constraint limits the amount of independent xy information which is contained in the measurements and tends to destabilize the problem. Our results were achieved by choosing well-constrained initial estimates of the xyz positions described below, by fixing the z component during the xy iteration, and by perturbing the FLIP positions independently of the transponder positions. Although the discussion of the general least-squares method was described in terms of measured and estimated travel times, the actual implementation described here was in terms of horizontal ranges. Describing the implementation in terms of the variables introduced in Eqs. (1) and (2), the model parameters $a_j, j = 1,N$ are the x and y positions of the FLIP transceiver and the three bottom transponders; these x and y positions define the horizontal projection of the slant range from a specified transponder to FLIP which is designated $\hat{v}_k$, $k = 1,M$. The measured travel times are converted to horizontal projections designated v_k, $k = 1,M$, using the sound-speed profile and the fixed z components as shown below. The number of horizontal projections, M, is 3 for the FLIP perturbations and 424 for the transponder perturbations.

The conversion from the time domain to the space domain is dependent on the sound-speed profile between the specified depths. Assuming a constant sound speed and therefore a straight-line path, and expanding the v_k's for illustrative purposes, the measured travel time is related to the xyz position as

$$\text{measured travel time} = \tfrac{1}{c}\,(\text{slant range}),$$

$$\text{slant range} = [(x_t - x_r)^2 + (y_t - y_r)^2 + (z_t - z_r)^2]^{1/2}, \tag{6}$$

$$\text{horizontal projections} = [(\text{slant range})^2 - (\delta z)^2]^{1/2}$$

$$= [(x_t - x_r)^2 + (y_t - y_r)^2]^{1/2},$$

$$v_k = \hat{v}_k,$$

where c is the sound speed, x_t, y_t, z_t represent the transmitter position, and x_r, y_r, z_r represent the receiver position. Sound speed is not constant in the ocean environment, and a varying sound-speed profile refracts acoustic energy; however, under certain conditions the harmonic mean, defined below, may be used with minimal error. To estimate the travel time differences due to refraction effects, the configuration parameters of the September experiment were specified and employed as inputs to the generic sonar model (GSM).[10] The GSM used generalized ray theory to calculate the ray path and travel time between a transmitter–receiver pair by assuming a sound-speed profile with layers of constant gradient. The simulation results are presented in Table I, which shows the travel time between an estimated transponder position and the array for a 12-kHz signal as a function of range, depth, and sound-speed profile. The first column (right of the double vertical bar) represents the results generated by assuming a constant sound speed of 1500 m/s throughout the water column. The second column was calculated using Eq. (8) shown below, with historical values of temperature and salinity versus depth for the area covering the experiment site and at the same time of year.[11] The third column used the harmonic mean, calculated by numerical integration of the layered sound-speed profile over depth to estimate travel time which is then converted to speed:

$$c = (z_T - z_0) \Big/ \int_{z_T}^{z_0} \frac{dz}{C(z)}. \tag{7}$$

The $C(z)$ profile used in the equation above is shown in Fig.

TABLE I. Sound-speed impact on travel time predictions.

Horizontal range (m)	Receiver depth (m)	Travel time versus sound speed, depth, and range: 4573-m source depth, 12 kHz GSM travel time predictions using Constant profile (1500 m/s) (s)	Historic profile (s)	Harmonic mean (s)	Deep ctd (s)
2000	90	3.2724	3.2740	3.2733	3.2733
2600		3.4546	3.4563	3.4556	3.4555
2000	400	3.0848	3.0839	3.0834	3.0833
2600		3.2774	3.2765	3.2759	3.2758
3000		...	...	3.4243	3.4241
5000		...	...	4.3387	4.3382
10000		...	...	7.2181	7.2152
2600	1600	2.6325	2.6184	2.6175	2.6174
2600	2800	1.0972	1.0726	1.0717	1.0716

3 and was calculated using the Unesco equations[12] relating conductivity to practical salinity, sound speed to salinity, temperature and pressure, and pressure to depth. The conductivity, temperature, and pressure measurements were obtained from a surface ship on Julian day 267 at 2243 GMT within 1 nmi. of the FLIP location. Sound-speed profiles in the ocean are typically very stable below the thermocline

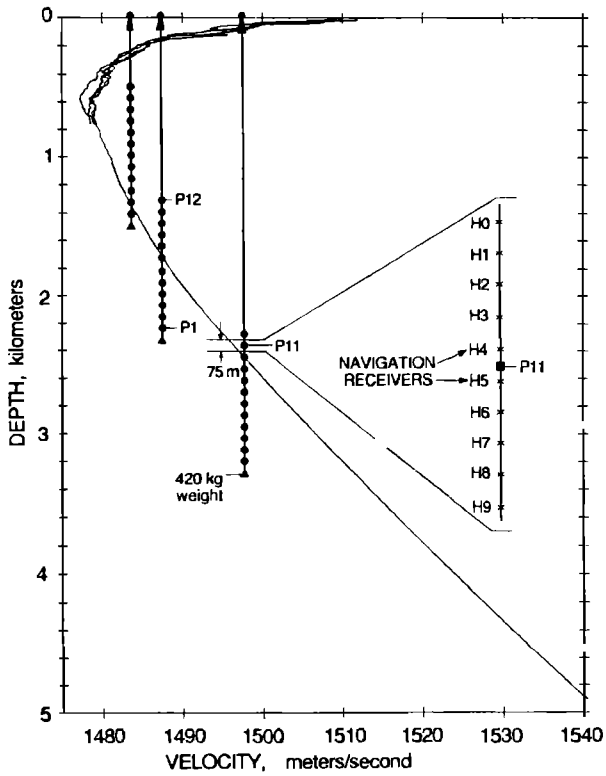

FIG. 3. Array navigation receivers and sound-speed profiles. The array was deployed at three nominal depths during the September 1987 experiment. The sound-speed profile is used in the conversion from travel times to spatial position. This profile was calculated from CTD data (0–4900-m depth) and is shown with three profiles calculated from XBT data (0–700-m depth) chosen to illustrate the variation in sound speed in the upper ocean layer. The navigation data from one receiver per array section (H5) were recorded during the experiment.

over the time period of the sea test. The diversity in temperature at the surface, however, imparts temporal variations in the sound-speed profile. Temperature measurements were acquired from expendable bathythermograph (XBT) casts deployed from FLIP twice a day throughout the experiment. Temperature data were converted to sound speed and decimated to maintain compatibility with program inputs. This conversion utilized historical salinity data[11] and was implemented by means of the following equation[13]:

$$c = 1449.2 + 4.6T - 0.055T^2 + 0.000\,29T^3 + (1.34 - 0.10T)(S - 35) + 0.016z, \quad (8)$$

where c = sound speed (m/s), T = temperature (°C), S = salinity(ppt), and z = depth(m). The maximum difference in the harmonic mean due to time variation in surface temperatures was about 1.5 m/s (0.1% of the mean speed). This affects the predicted travel time from a transponder to a receiver at 90 m by about 3 ms (5 m). An error in the sound-speed correction of the measurements translates into a larger array element rms error, but does not substantially affect the estimated position due to the nearly equilateral triangle system configuration. Due to possible inaccuracies in the absolute XBT measurements, and the robust nature of the system configuration to errors in sound speed, the profile was considered constant over time and equal to the CTD calculations. The fourth column in Table I incorporates refraction effects due to changes in the sound-speed profile $C(z)$ described above. The predictions generated by the GSM indicate that, for the geometrical configuration of the September experiment shown in Fig. 4, the error in travel time by assuming a straight-line path with a constant average sound speed is 0.1 ms; therefore, using the harmonic mean of the sound-speed profile introduces a negligible error (0.15 m) in the array positions.

GPS satellite positions at FLIP and the surface ship during transponder deployment provided the initial estimates of the transponder xy positions to within tens of meters. The clement weather that prevailed during the deployment and the negative buoyancy of the transponders (sink rate of ≈ 1 m/s) constrained the final transponder positions. Initial

transponder depths were estimated by subtracting the transponder anchor line length from the echo-sounding depth measured at FLIP. The assumption that the seafloor is flat in the immediate area of FLIP was corroborated by bottom-mounted Swallow floats deployed approximately 2 nmi from FLIP. Preliminary Swallow float depth estimates were within 15 m of the depth measured at FLIP.[14]

Once the ingredients for the least-squares method have been accumulated, the xy positions are adjusted until the root-mean-squared (rms) error satisfies the convergence criteria described below. This is accomplished in several steps by first maintaining constant transponder positions and perturbing the FLIP positions to minimize errors, then holding the current FLIP positions constant while perturbing the transponder positions to minimize errors, then examining the mean-squared error of each FLIP position to determine (via a user parameter) whether it should be preserved as a viable contributor, and, finally, repeating the entire procedure until the convergence criteria are satisfied. The perturbation adjustment is calculated with the search direction $\mathbf{p}$ defined as the negative gradient. The step size is a constant (1.5 m) unless the rms error is less than 1 m, at which time the step size begins to decrease; as the minimum is approached, the step size is calculated as a function of the percent change in iterated rms error. The convergence criteria are defined as follows: an absolute rms error less than 0.15 m, a 0.15% change in the iterated rms error, or a maximum of 30 iterations. A typical number of loop iterations required for the convergence of the September data set were 3 for each inner loop and 5 for the entire procedure, the repetition factor depending on the user parameters. A detailed description of the software implementation and its usage is documented.[4]

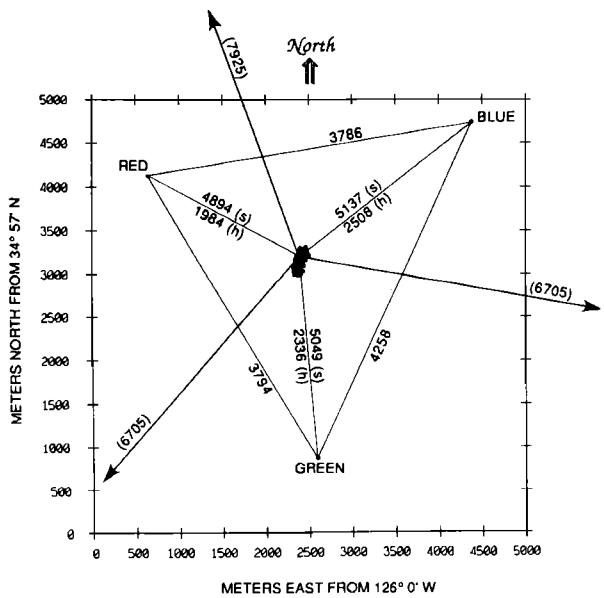

FIG. 4. Spatial configuration for navigation during the September 1987 sea test. The estimated positions of FLIP and the three bottom transponders (red, green, and blue) measured hourly over 18 days are shown in plan view. The FLIP mooring lines are represented by arrows, and the slant range (s) and horizontal projection of the slant range (h) are indicated in meters from an arbitrary FLIP xy position (2400, 3200). Transponder baseline distances are indicated in meters.

The transponder depths were iterated manually by minimizing the magnitude and dispersion of rms error across the array. Increasing rms errors across the array was shown by the simulations in the following section to be an indication of potential transponder depth error. The FLIP database used to navigate the transponders was sampled during tidal peaks to discern whether there was any transponder movement due to tidal forces. No appreciable difference was observed, and transponder movement is assumed to be negligible.

2. FLIP and array element localization

The localization procedure for FLIP and the array is essentially the same as just described for the transponders. With the transponder positions known, the FLIP and array element navigation may be calculated in real time.

The initial xy positions for FLIP and the array elements were estimated from GPS positions after FLIP was moored (Julian day 255). Because FLIP's position was maintained by a three-point moor, the same initial xy position was used for each FLIP position throughout the test. If the initial xy position must be estimated without GPS, or if the receiver is not moored, a geometric estimate may be obtained from the transponder slant ranges. The depths of the array elements were measured to within 1.5 m by the 12-kHz transmitter mounted on the bottom of FLIP. The 12-kHz signal was received by each navigation receiver without exception; however, there were indications of slight interference in the variability of the arrival time of the resulting correlated output. The array was deployed under 420 kg of tension to maintain verticality and constrain the depth parameter. A 1.5-m error in array depth, because this input is a fixed parameter in an equilateral configuration, translates into less than 0.5 m of error in the xy positions of the array, but changes the rms error by as much as 2.5 m.

The noise in the travel times measured at the array is greater than the noise in the hand-picked data measured at FLIP. To improve the data quality, various averaging, thresholding, and interpolation schemes were incorporated in the processing software. Should a receiver not detect a return, or if the detected return is not within specified thresholds for range and depth variability, various interpolation/extrapolation software options may be specified. Prior to the least-squares iterations, the data may be smoothed with a running average filter. The travel time measured at the array represents the time from FLIP to the transponder to the array. Therefore, to acquire the transponder-to-array travel time required by the least-squares procedure, the FLIP-to-transponder travel time (measured at FLIP once an hour) is interpolated and subtracted from the travel time measured at the array (approximately once per minute).

C. Simulations

Simulations were conducted to examine the array position sensitivity to errors in the transponder and FLIP positions. The spatial configuration shown in Fig. 4 simulates the September sea test; FLIP is centrally located in the transponder network (identified by colors), and the array is di-

rectly under FLIP. The transponders, FLIP, and the array are initially assigned to known positions with slant ranges as shown. Individual transponder positions were perturbed, and the resulting array shape and relative errors were examined. These tests were conducted first with the array in a vertical orientation; that is, the array element xy positions were identical to those of FLIP, and then with the array straight but tilted 2° vertically at 225° azimuth. Zero mean Gaussian random errors ($\sigma^2 = 3$ m) were added to the array travel times with no appreciable changes. The final simulation configuration perturbed the FLIP position. Because the array measures travel times of rays which originate at FLIP, errors in the FLIP parameters map into array positional errors.

The simulations provide an understanding not only of the error magnitudes but also of their dispersion across the array. With a + 25-m perturbation in the x or y transponder positions, the effect on the initially vertical array is a horizontal translation in the direction of the transponder with no relative array positional errors. If an error is introduced in the z transponder position, the array is translated and tilted. Figure 5(a) shows the effect on the array as the blue transponder is perturbed by 100-m errors individually in x, y, and z, and finally simultaneous 100-m errors in x, y, and z. Figure 5(b) shows the effect of transponder depth errors. Each transponder depth was increased and decreased individually by 10 and 25 m. The dot in the center of the figure is the navigated FLIP and array positions with no input errors; with a decrease in transponder depth, the input slant range appears to be too long, and the array is translated in a direction away from the transponder (notated by O's on the plot) and tilted slightly. An increase in transponder depth operates similarly except in a direction toward the transponder (notated by ×'s on the plot). The results of the simulations for the positive perturbations with an initially straight vertical array are compiled in Table II. The columns indicate which parameter has been perturbed and the amount of the perturbation, the translation and percent change in range calculated for the FLIP position, system tilt, and position rms [$\sqrt{F}$ in Eq. (1)]. The rms error is shown as a single number if the difference in error across the array was less than 0.1 m; when two numbers are shown, they indicate the error at FLIP and the bottom element of the array. By examining the FLIP translation and rms error for the x and y perturbations in Table II, it is clear that the x position is controlled by the red and blue transponders, and the y position is controlled by the green and blue transponders (Fig. 4). The difference in rms error between the three transponders reflects the percent deviation from original slant range. The dispersion in rms error was used to iterate the transponder depth. This can be seen, for example, in the results of the red depth perturbation which yields an rms error at FLIP of 18.13 m, monotonically decreasing to 13.48 m at the bottom of the array. The array and FLIP positions are more sensitive to errors in transponder depth (60%–70% of perturbation) than to errors in transponder horizontal (xy) position ($<35\%$ of perturbation). To demonstrate this sensitivity dichotomy, with FLIP at a known position x,y from a transponder, the FLIP translation T_z due to an error δ_z in transponder depth, and the translation T_{xy} due to errors δ_x and δ_y in transponder xy position are

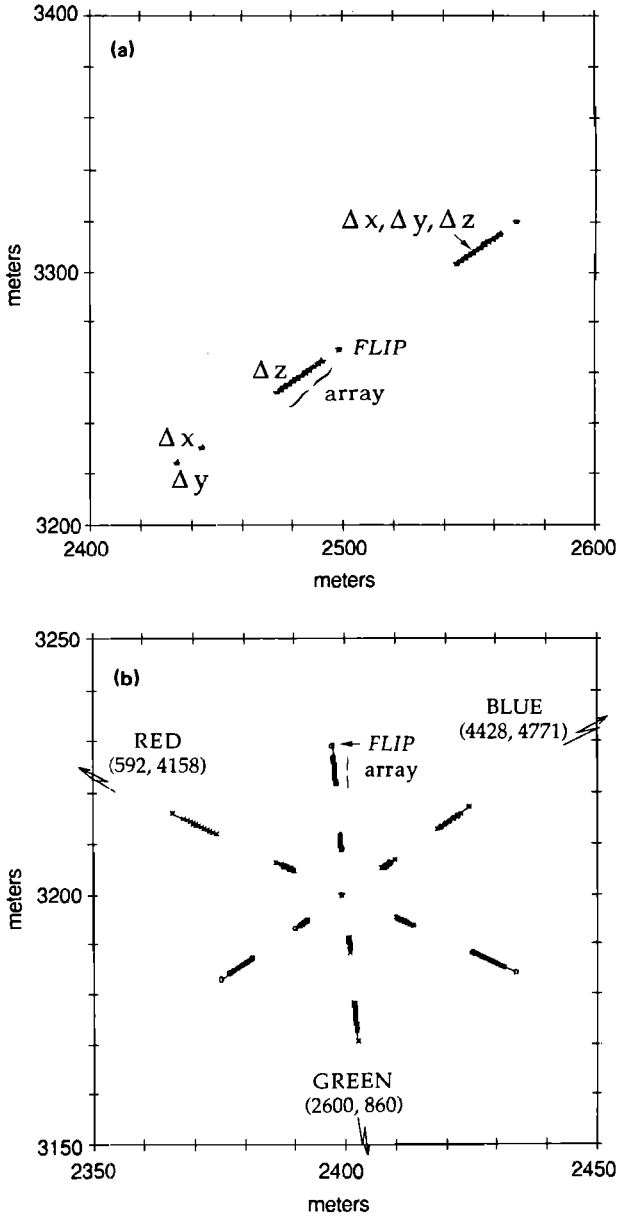

FIG. 5. Error simulation results. The effect of errors in the transponder positions on the shape and position of FLIP and the array are shown in plan view. (a) Effect on the FLIP and the array as the blue transponder is perturbed in x, y, and z. (b) FLIP and array positions as a function of transponder depth error.

$$T_z = h - s\sin\{\cos^{-1}[(d+\delta_z)/s]\}, \tag{9}$$

$$T_{xy} = h - [(x-\delta x)^2 + (y-\delta y)^2]^{1/2}, \tag{10}$$

where h and s are the horizontal and slant ranges, respectively (Fig. 4), d is the difference in depth between the base of FLIP and the transponder, x is the component of h in the $\hat{x}$ direction, and y is the component of h in the $\hat{y}$ direction. FLIP is constrained by the experimental configuration to move approximately along the line defined by the horizontal projection of the slant range between the perturbed transponder position and FLIP (Fig. 5). To quantify these translational errors, a δ_z of + 25 m in the red transponder depth

TABLE II. Navigation error simulations.

Perturbation (m)	% change in slant range	% change in horizontal range projection	Array tilt (deg)	Translation from initial position (m)	rms error (m)	% of original perturbation
		FLIP and array position with errors in transponder positions				
Red $X+25$	0.1323	0.7780	0.000	15.802	7.11	28.4
Green	−0.0693	−0.3095				
Blue	−0.0724	−0.2940				
Red	0.0110	0.0640	0.000	1.498	0.78	3.1
Green $X+25$	−0.0124	−0.0550				
Blue	0.0012	0.0049				
Red	0.0576	0.3333	0.000	14.161	6.45	25.8
Green	0.0636	0.2832				
Blue $X+25$	−0.1360	−0.5463				
Red $Y+25$	−0.0638	−0.3663	0.000	7.540	3.83	15.3
Green	0.0383	0.1708				
Blue	0.0296	0.1198				
Red	−0.0669	−0.3880	0.000	15.849	8.73	34.9
Green $Y+25$	0.1468	0.6636				
Blue	−0.0879	−0.3567				
Red	0.0454	0.2627	0.000	11.149	5.01	20.0
Green	0.0499	0.2223				
Blue $Y+25$	−0.1069	−0.4304				
Red $Z+25$	−0.3083	−1.8163	0.483	37.199	18.13, 13.48	72.5, 53.9
Green	0.1778	0.7907				
Blue	0.1624	0.6567				
Red	0.1405	0.8112	0.375	29.320	16.63, 12.39	66.5, 49.6
Green $Z+25$	−0.2689	−1.2156				
Blue	0.1489	0.6022				
Red	0.1225	0.7076	0.382	30.631	14.46, 10.76	57.8, 43.0
Green	0.1419	0.6311				
Blue $Z+25$	−0.2901	−1.1915				
		FLIP and array positions with errors in FLIP slant ranges				
Red $+25$	0.3561	2.0453	0.424	41.936	19.04, 15.73	76.2, 62.9
Green	−0.1865	−0.8346				
Blue	−0.1855	−0.7543				
Red	−0.1454	−0.8450	0.315	33.396	18.28, 15.20	73.1, 60.8
Green $+25$	0.3122	1.3848				
Blue	−0.1780	−0.7236				
Red	−0.1279	−0.7432	0.315	34.034	16.08, 13.51	64.3, 54.0
Green	−0.1577	−0.7054				
Blue $+25$	0.3284	1.3250				

of Eq. (9) resulted in a 58-m FLIP xy position translation, and a δ_x of $+25$ m in the red transponder x position of Eq. (10) resulted in a FLIP xy position translation of only 22 m, illustrating that FLIP position is more sensitive to errors in transponder depth than to errors in transponder xy position.

An error in transponder position, when the array is tilted, will distort the vertical and azimuthal array orientation as well as impart a horizontal translation. A tilted array will show a horizontal translation comparable to the initially straight array, but with azimuthal and vertical rotations. The vertical angular change is similar to that of the straight array for depth perturbations and small but noticeable for horizontal perturbations. The azimuthal angular change is larger for both horizontal perturbations (0.3° tilt) and depth perturbations (14° tilt).

An error in a FLIP slant range also translates into an array positional error. An error which increases the slant range moves FLIP away from the transponder and the array closer. It also induces a tilt in the array making the bottom closer to the no-error position than the top, with a corresponding decrease in rms error from the top to bottom of the array. Table II shows the results of the simulation for $+25$-

m errors in the three transponder slant ranges to FLIP. A transponder slant range error δ_s before iteration creates a translation error:

$$T_s = h - \sqrt{h^2 - 2\delta_s s - \delta_s^2}, \tag{11}$$

where h and s are defined above. An error δ_s of $+25$ m in the red transponder slant range of Eq. (11) yields a translation error T_s of 62.3 m prior to iteration.

These simulations quantify the mapping of errors in slant ranges to errors in xy positions. The adjustment direction is dictated by the measurement direction (horizontal range direction) not the model parameters (xy directions) or the error direction. The positions of FLIP and the array are more sensitive to errors in transponder depth and FLIP slant range than to errors in transponder horizontal position. This sensitivity is attributed to the constraint of fixed array depth (negligible measurement errors) necessitating an assignment of the error to the horizontal projection. These errors are magnified and dispersed across the array. It was this dispersion that was used as a criteria for convergence during the transponder depth iteration.

III. DATA ANALYSIS

The motions of FLIP and the array are analyzed to determine the navigation accuracy, the extent of movement, and possible forcing functions driving the system. The data consisted of the GPS satellite positions acquired at FLIP, estimated FLIP positions spanning a period of 18 days with 1-h samples, and estimated array element positions at a nominal depth of 850 m spanning a 24-h period. The GPS positions acquired aboard FLIP provide an independent verification of the estimated FLIP positions derived using the least-squares method (Fig. 6). The GPS positions in latitude and longitude were converted to meters from the least-squares origin by calculating the local radius of the earth as follows[15]:

$$x_{\mathrm{GPS}} = r_{\mathrm{pos}}\,\delta(\mathrm{lat}), \quad y_{\mathrm{GPS}} = r_{\mathrm{pos}}\cos(\mathrm{lat})\,\delta(\mathrm{long}), \tag{12}$$

where

$$r_{\mathrm{pos}} = r_{\mathrm{eq}}\,[1 - f\sin^2(\mathrm{lat})], \qquad f = \frac{r_{eq} - r_{\mathrm{polar}}}{r_{\mathrm{eq}}}$$

and where x_{GPS} is the E–W distance, y_{GPS} is the N–S distance, r_{pos} is the earth's radius at the position latitude, $\delta(\mathrm{lat})$ is the difference in latitude between the position and the origin, $\delta(\mathrm{long})$ is the difference in longitude, lat is the latitude of the position, r_{eq} is the earth's equatorial radius, and r_{polar} is the earth's polar radius. The observed 10-m rms deviation between the GPS and navigated FLIP positions is reassuring. FLIP positional errors are independent and distributed normally at a χ^2 0.05 level of significance with zero mean and a standard deviation of 1.1 m. Array positional errors may deviate from a normal distribution, depending on the nature of the transponder and receiver errors; however, considering a receiver with low errors, a Gaussian distribution of 2.9-m mean and 0.81-m standard deviation may be compared at a 0.05 level of significance. Receiver detection threshold mismatch, tuned filter drift, sound-speed errors,

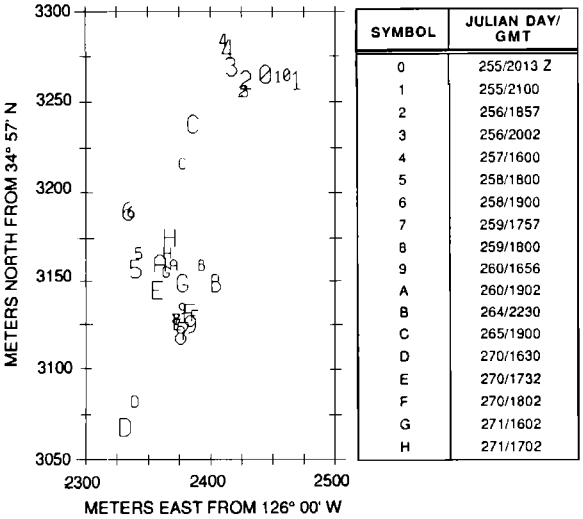

FIG. 6. Comparison of GPS satellite and acoustic navigation. FLIP GPS positions are compared to those estimated by the least-squares navigation. The large symbols represent the GPS positions, while the corresponding small symbols represent the estimated FLIP positions. A bias correction, attributed to drift of the transponders during deployment, of 24.5 m was added to the N–S estimated positions and 1.2 m to the E–W estimated positions.

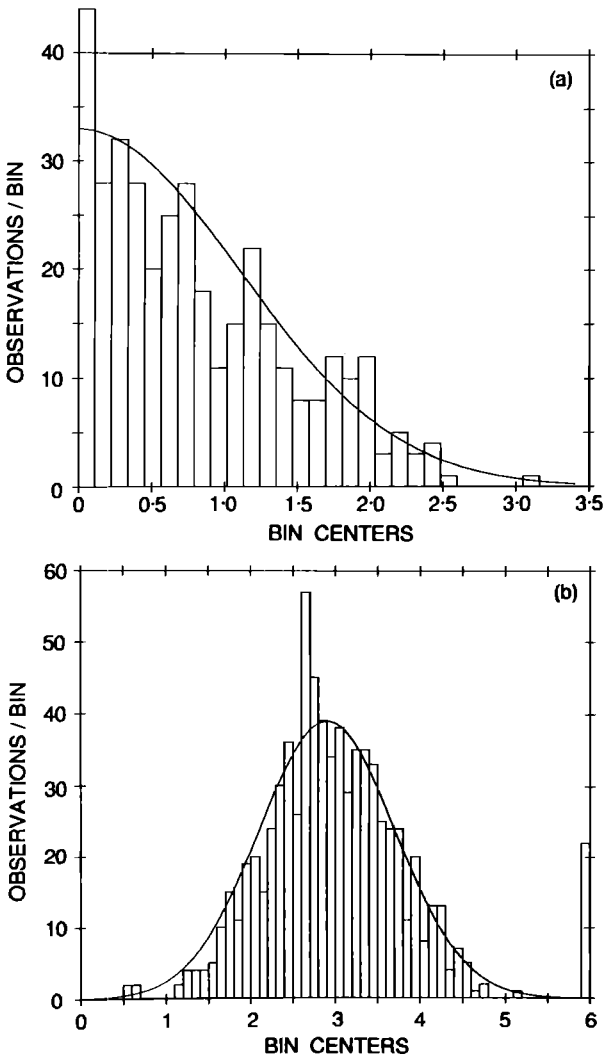

FIG. 7. Error distributions. The error distributions shown for (a) FLIP and (b) array navigation receiver No. 8 are independent as illustrated by a runs test and Gaussian at a 0.05 level of significance. The high transponder errors shown in the 6-m bin of (b) are due to transponder detection of multipath propagation.

the FLIP position, as described earlier, contribute to the mean. FLIP and array error distributions are shown in Fig. 7.

The motion of FLIP (Fig. 8) is primarily controlled by the local wind field, the tides, and the tension on the mooring lines. The low-frequency movement of FLIP is driven by the local wind, primarily from the north during the entire experiment. The wind speed has a high negative correlation with FLIP N–S positions and, to a lesser extent, with FLIP E–W positions. This is expected as a northerly wind would tend to push FLIP toward the south. At 35° N latitude the tidal cycle is semidiurnal and appears as a prominent component in the FLIP time series. The tidal component in the E–W displacement lags 2 h behind the N–S component, producing a clockwise rotation. This rotation is also seen in the calculated tidal velocity ellipse (Fig. 9), which lags the displacement by 90°. The tidal velocity ellipse, which includes contributions from both the barotropic and baroclinic modes, is comparable to simultaneous estimates of the current field recorded by current meters deployed at 50 and 100 m below the water surface from FLIP. Although the current meter measurements are relative to FLIP, the tidal component is four times as strong as the constrained FLIP component and leads in phase due to FLIP's massive structure and mooring line effects.

The motion of the array (Fig. 10) is controlled by the tides, the motion of FLIP, and possibly by internal waves or higher frequency surface motion that is unresolved in the FLIP data set. The longest period movement of the array was on the order of days and was driven by FLIP's response to the wind. This is inferred by the fact that the top array position was normally within a 30-m horizontal slant range of FLIP which traveled over 300 m during the 18 days (within 20 m in Fig. 11). The tidal cycle is evident as a 12-h oscillation in the 24-h time series and as the 0.083-cycles/h peak in the spectrum (Fig. 12).

Higher frequency array oscillations appear in the expanded time series in Fig. 10(c) and (d), but are not stationary over the 24 h, and all but disappear from the spectrum during the averaging process. Although the sample-to-sample motion of the array is on the same order as the errors, the errors are independent and Gaussian; therefore, we believe the fluctuations which occur with periods from 15 or 20 min to 2 h are due to array motion. Modeling the array as a simple pendulum where the center of mass is derived from four component parts (uplink wire, array, kevlar, and weights), the natural period of oscillation is just over 1 min. The damped natural period for a velocity of 5 cm/s is 7 min with a damping coefficient of slightly less than critical. These periods do not coincide with the 0.3–2-h periods seen in the array data; therefore, the high-frequency motions must be due to environmental forcing functions. We believe it to be a combination of two processes: the coupling of the array to the surface and the array response to low-order modes of the internal wave field. The motion whose periods are from tens of minutes to many hours (Väisälä frequency in the N Pacific is about 20 min near the surface) and whose horizontal velocities of 1–2 cm/s are reasonable for a constrained internal wave response[16] where typically horizontal currents are about 5 cm/s and horizontal current spectra is

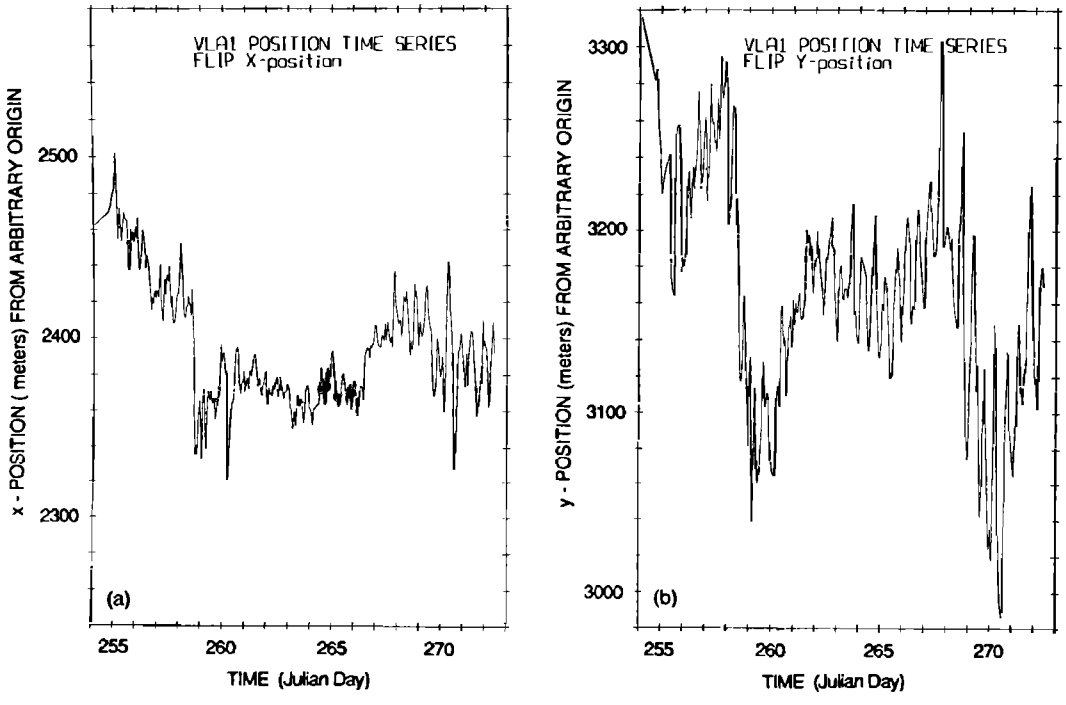

FIG. 8. FLIP position time series. The FLIP positions are estimated approximately every hour and plotted over the 18-day experiment. The (a) x positions, increasing toward the east, and the (b) y positions, increasing toward the north, are plotted on the same relative vertical scale, but with different origins.

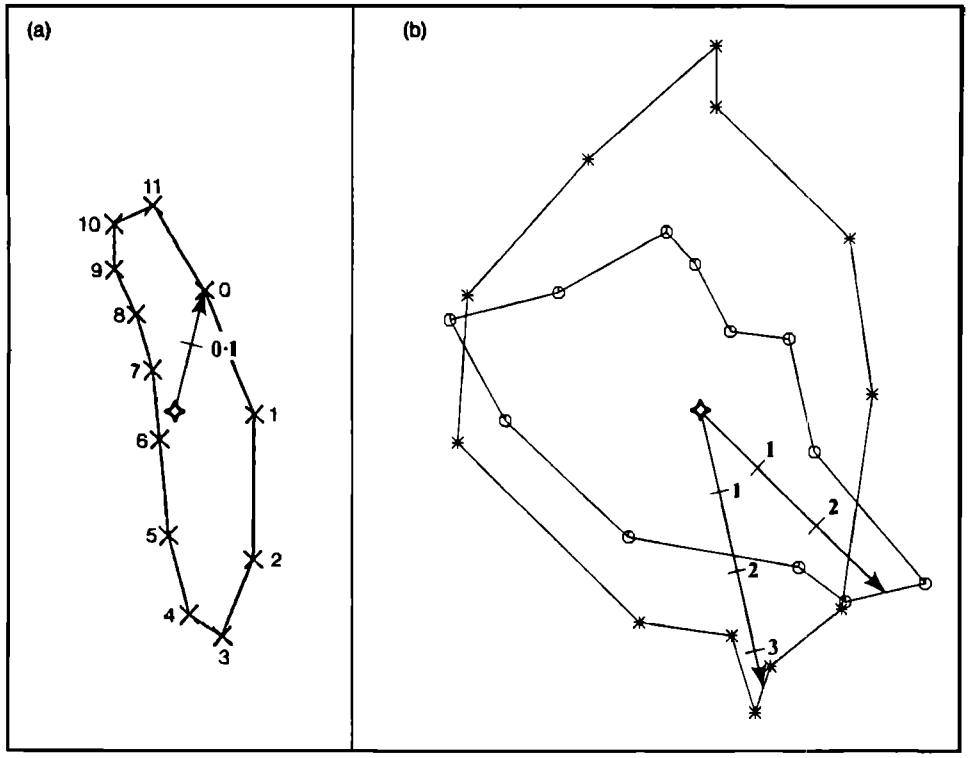

FIG. 9. Tidal current ellipse. (a) The current ellipse estimated from FLIP positions was calculated by finite differencing the 18-day time series, low-pass filtering the resulting hourly estimates, and then averaging 12-h segments. The tips of the current vectors were plotted from a common origin every hour. The 0 GMT vector is marked in cm/s. (b) Current meter data collected from FLIP represent 12-h segment averages (O) over 13 days at 43 m and (*) over 20 days at 90 m. Mean velocities of 7.5 cm/s E, 0.64 cm/s N at the 43-m site, and 7.2 cm/s E, −0.91 cm/s N at the 90-m site were removed.

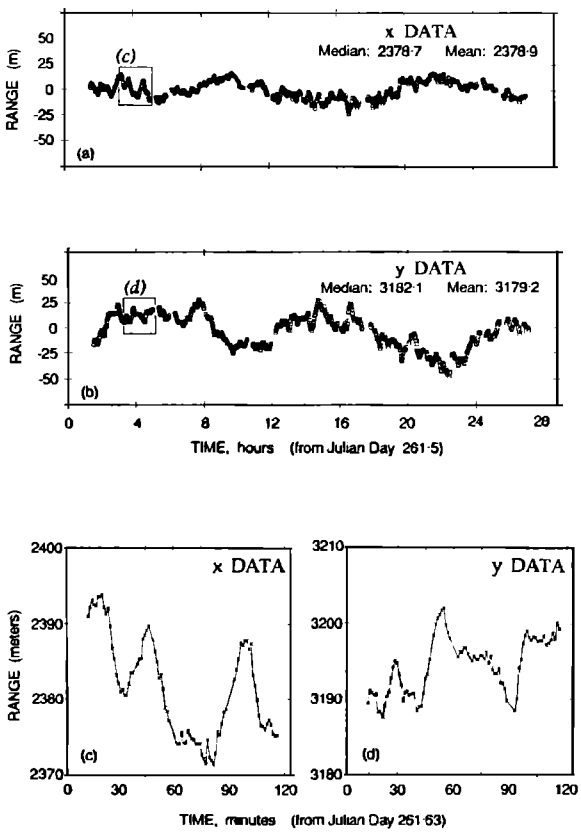

FIG. 10. Array position time series. The estimated positions for the array section 8 navigation receiver are plotted relative to the median value. In (a) range increases toward the E, and in (b) toward the N. The area identified by a box in (a) and (b) is expanded in (c) and (d) to illustrate this high-frequency motion.

dominated by the lower-order modes.[17] The motion spectrum does not show a peak at the local inertial frequency,[18] nor an ω^{-2} energy dependency between the inertial frequency (0.048 cycles/h) and the Väisälä frequency common in internal wave energy spectra.[19] This characteristic shape is apparently filled in by the coupled response to surface-generated motions.

The array shape during the experiment is modeled to first order as linear, but slightly tilted from vertical. The array shape plotted approximately every 3 min over the first hour of data shown in Fig. 10(c) and (d) is illustrated in Fig. 11, where the horizontal deformation has been exaggerated for clarity, extending 50 m in the horizontal compared to 1600 m in the vertical. These data show a linear array with receiver position deformations within the rms error estimated by the least-squares procedure[4]; and with a deviation of less than 5 m across the array aperture, the array maintains a vertical orientation to within 0.5°. Array shape snapshots every 5 h over a longer period of time (20 h) show that the array follows FLIP to within a 30-m horizontal range (Fig. 13). The change in array depth due to such a 30-m deviation, assuming a linear cable, is only 1 m, which is not significant. The array tilt from vertical is within about 1°, considering the maximum deviation (15 m) shown across the aperture. The linear pendulumlike response is particularly apparent in the 2-min snapshots as the array responds to the motion of FLIP and the internal wave field. Although the time sequence of the individual estimates is not legible, the crossing uplink lines indicate small-scale array oscillations, through which the linear shape is maintained. It is evident that the array exhibits a more active response (presumably due to

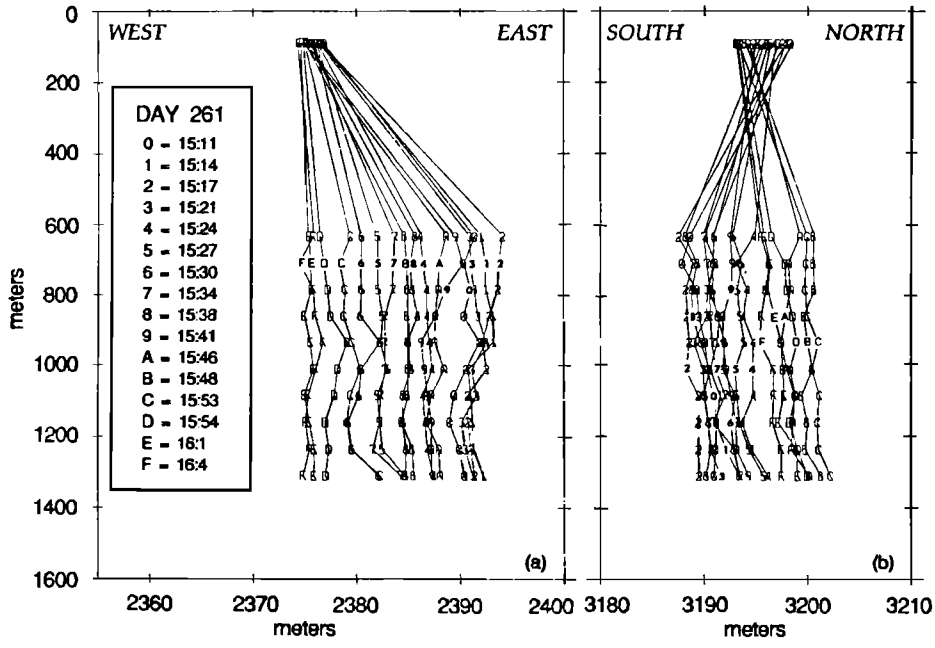

FIG. 11. Array shape over 1 h. The positions of the ten deepest navigation receivers are shown over a 1-h period. The top two receiver positions were deleted due to their large errors (Ref. 4). The two views are (a) East–West versus depth, and (b) North–South versus depth. The snapshots are spaced at approximate 3-min intervals and represent a subset of the data shown in Fig. 10(c) and (d).

internal waves) than FLIP by examining the extent of FLIP motion compared to that of the array during the same time period. The array moves over four times the E–W distance covered by FLIP during the hour plotted in Fig. 11.

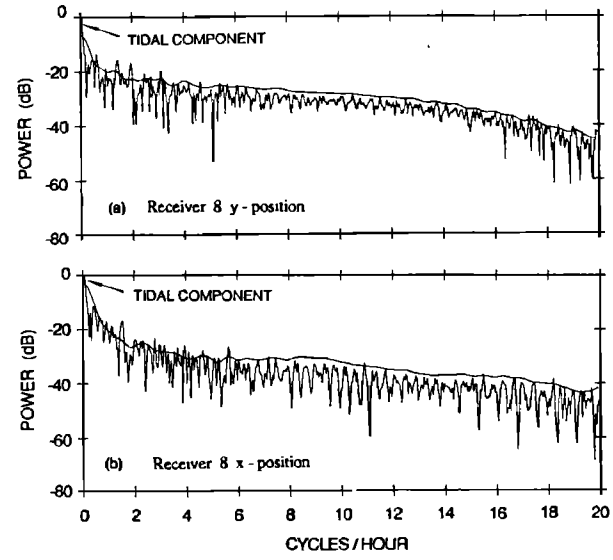

FIG. 12. Spectrum of array motion. For receiver (a) x position and (b) y position, the smooth curve is an averaged 1024-pt spectrum of 15, 50% overlapped, Kaiser–Bessel windowed ($\alpha = 2.5$) 128-point time series plotted on a relative scale. A single spectrum was computed similarly over the entire time series and plotted on the same relative scale with 0.039-cycles/h resolution for more accurate identification of the narrow-band spectral components.

IV. CONCLUSION

The least-squares method was implemented to convert measured travel time data to spatial positions for FLIP and a 900-m vertical array by assuming a harmonic sound speed and normally distributed errors. Navigated FLIP positions (mean = 0.5 m, $\sigma = 1.1$ m) agree with positions obtained from GPS satellite navigation to within an rms error of 10 m. A mean error as small as 2.8 m with a standard deviation of 0.8 m was obtained for array element position; however, each receiver displayed a unique error distribution due to variations in the array detectors. Array positions were found to be particularly sensitive to errors in FLIP position and transponder depth. This was demonstrated by simulation to be a result of the optimization constraints. Iteration of array depths and incorporation of a more accurate sound-speed correction has shown promising preliminary results by reducing the mean rms array element error to less than 1 m, while leaving the estimated positions within 0.2 m of the positions presented here. The navigated positions are tied to an absolute frame of reference using transponder GPS locations, and the absolute positions are substantiated by the GPS positions at FLIP and the high negative correlation between FLIP's N–S component and the wind speed. FLIP's position was driven by the winds and tides, but was constrained to approximately a 300-m range by a three-point mooring. The array position was driven by tidal motions at a semidiurnal period, and apparently by internal waves and coupled surface-wave motion at higher frequencies. Array high-frequency motions were up to a factor of 4 larger than FLIP motions, although the array normally maintained a vertical orientation to within a tilt angle of 2° and remained within a 30-m range of FLIP.

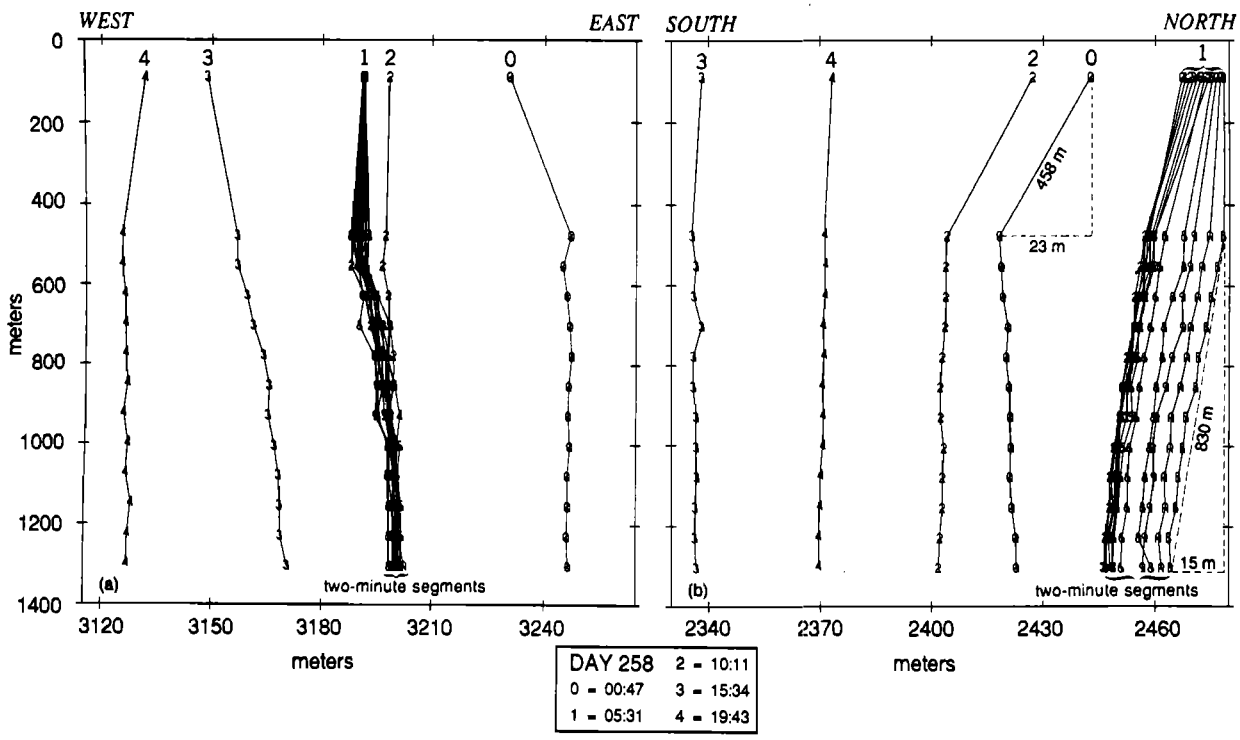

FIG. 13. Array shape over 20 h. The positions of the 12 navigation receivers are shown at 5-h intervals over a 20-h period. The two views are (a) East–West versus depth and (b) North–South versus depth. Snapshots every 2 min are shown beginning at 5:31 GMT over a 24-min period.

ACKNOWLEDGMENTS

The authors are indebted to C. de Moustier for his review of the manuscript and W. Hodgkiss, S. Flatte, K. Watson, and G. D'Spain for their valuable suggestions. We thank F. V. Pavlicek for engineering expertise, E. Wolin, P. Henkart, R. Currier, C. Lowenstein, and R. Lawhead for software support, A. Aja, D. Ensberg, and P. Scott for their assistance in data processing, and J. Griffith for her illustrative talents. The captain and crew of the research platform FLIP contributed to the sea-going operation. This work was supported by the Office of Naval Research under Contract N00014-87-K-0225 and N00014-87-C-0127.

[1]B. J. Sotirin and J. A. Hildebrand, "Large aperture digital acoustic array," IEEE J. Ocean. Eng. **OE-13**, 271–281 (1988).

[2]F. N. Spiess, "Panel on Ocean Bottom Positioning and National Research Council Committee on Geodesy," in *Seafloor Referenced Positioning: Needs and Opportunities* (National Academy, Washington, DC, 1983), p. 15.

[3]D. E. Boegeman, private communication (1988).

[4]B. J. Sotirin and W. S. Hodgkiss, "Navigation software for the MPL vertical line array," MPL TM-409, Marine Physical Laboratory, Scripps Institution of Oceanography, University of California, San Diego, CA (March 1989).

[5]P. E. Gill, W. Murray, and M. H. Wright, *Practical Optimization* (Academic, Orlando, Fl, 1981), p. 100.

[6]G. L. Duckworth, "A robust algorithm for tracking of drifting acoustic arrays in the arctic," Signals, Systems and Computers, 21st ASILOMAR Conference Proceedings, Pacific Grove, CA (2–4 Nov. 1987).

[7]H. W. Sorenson, *Parameter Estimation—Principles and Problems* (Dekker, New York, 1980), pp. 45, 225.

[8]F. N. Spiess, "Analysis of possible sea floor strain measurement system," Mar. Geod. 9 (4), 385–398 (1985).

[9]W. Smith, W. M. Marquet, and M. M. Hunt, "Navigation transponder survey: design and analysis," in *Oceans 75 Record* (IEEE, San Diego, CA, Sept. 1975), pp. 563–567.

[10]H. Weinberg, "Generic sonar model," NUSC TD-5971D, Naval Underwater Systems Center, New London, CT (1985).

[11]J. Churgin and S. J. Halminski, "Temperature, salinity, oxygen and phosphate in waters off the United States, Eastern North Pacific," National Oceanographic Data Center, Washington, DC (1974), Vol. 3.

[12]N. P. Fofonoff and R. C. Millard Jr., "Algorithms for computation of fundamental properties of seawater," Technical Paper 44, Unesco Division of Marine Sciences, Paris, France (1983).

[13]C. S. Clay and H. Medwin, *Acoustical Oceanography: Principles and Applications* (Wiley Interscience, New York, 1977), p. 3.

[14]W. S. Hodgkiss and G. L. D'Spain, private communication, (1988).

[15]R. A. Stacey, *Physics of the Earth* (Wiley, New York, 1976), p. 74.

[16]C. Garrett and W. Munk, "Internal waves in the ocean," in Annu. Rev. Fluid Mech. (Annual Reviews Inc., 1979), 339–369.

[17]R. Pinkel, private communication (1989).

[18]W. Munk, "Internal waves and small-scale processes," in *Evolution of Physical Oceanography* (MIT, Cambridge, MA, 1981), pp. 264–291.

[19]J-H Hu and P. P. Niiler, "NEPAC current meter and XBT data for circulation in NE Pacific thermocline," SIO Ref. No. 87-4, Scripps Institution of Oceanography, University of California, San Diego, CA (Feb. 1987).